Effect of QWR Shape on the Induced Elastic and Piezoelectric Fields

E. Pan[1] and X. Jiang[1]

Abstract It is of great importance to understand the factors that contribute to the strain and electrical distributions, which are induced by the misfit strain between a buried quantum wire (QWR) and its surrounding matrix. One of the important factors is the shape or geometry of cross section of the QWR. Utilizing a recent exact closed-form solution [Pan (2004)], we study the model system of QWRs with different shapes and calculate both the surface and internal elastic and piezoelectric fields induced by QWRs embedded in semiconductor GaAs substrates by properly setting the size and location of the QWRs. The effects of the QWR shape as well as the material orientation and free surface of the substrate on the elastic and piezoelectric fields are clearly demonstrated. Key conclusions are also drawn.

keyword: misfit strain, QWR, shape effect, exact closed-form solution, elastic and piezoelectric fields.

1 Introduction

Much research effort has been made during recent years on quantum heterostructures where quantum mechanics effects appear, thus providing rich opportunities for the design of novel devices. For example, semiconductor lasers could be improved by using two dissimilar materials as active and cladding layers [Lin (2001)] for promising applications as semiconductor light-emitting and laser diodes. Using quantum nanostructure, namely quantum well (QW), quantum wire (QWR), and quantum dot (QD), as active layers leads to even better laser performance [Lin (2001); Grundmann, Stier, and Bimberg (1994); Fu, Zhao, Ferdos, Sadeghi, Wang, and Larsson (2001); Shim, Choi, Jeong, Vinh, Hong, Suh, Lee, Kim, and Hwang (2002); Martinet, Dupertuis, Reinhardt, Biasiol, Kapon, Stier, Grundmann, and Bimberg (2000)]. Recently, the strained nanostructures have drawn considerable attention since the misfit strain can lead to the change in the conduction/valance bands which, in turn, together with the dimension confinement, alters the electronic and optical properties of the semiconductor structures [Notomi, Hammersberg, Weman, Nojima, Sugiura, Okamoto, Tamamura, and Potemski (1995); Lelarge, Constantin, Leifer, Condo, Lakovlev, Martinet, Rudra, and Kapon (1999); Medeiros-Ribeiro (2002); Martinet, Dupertuis, Reinhardt, Biasiol, Kapon, Stier, Grundmann, and Bimberg (2000); Constantin, Martinet, Leifer, Rudra, Lelarge, Kapon, Gayral, and Gerard (2000)]. For instance, the strained QWR can acquire a wavelength range not accessible with lattice-matched materials [Grundmann, Stier, and Bimberg (1994)].

For QWR structures, much work has been done to explore the effect of QWR shapes on various properties. Vargiamidis and Valassiades (2002) investigated the dependence of the quantized conductance of electron transport on the shape of QWR cross section with the existence of defects or impurities. Their work is stimulated by a previous research of Bogachek, Scherbakov, and Landman (1997), who took both the area and shape of the QWR cross-section (or nanowire) into consideration. While Anthony and Kelly (1994) studied analytically the effect of the cross-section geometry of the QWR on confinement energies, Thilagam (1997) performed analysis of the QWR cross-section on the exciton binding energy. Tsetseri and Triberis (2002) analyzed the effect of QWR shape on the ground state in QWR structures using finite difference method, whilst Ogawa, Itoh, and Miyoshi (1996) used finite element method to study the effect of geometric shape on the valence band of QWR.

Shape effect has been intensively studied not only numerically but also experimentally. By measuring the photoluminescence (PL) of four different geometries, i.e., rectangular, triangular, trapezoidal, and polygonal ones, Shim, Choi, Jeong, Vinh, Hong, Suh, Lee, Kim, and Hwang (2002) found that the highest light emission efficiency and best reproducibility in intensity and wavelength were associated with trapezoidal QWs. Likewise, Cheong, Choi, Suh, and Lee (2003) proved that trapezoidal QWs excel rectangle QWs as active materials to improve performance in

[1] Dept. of Civil Engineering, The University of Akron, Akron, OH 44325-3905.
E-mail: pan2@uakron.edu

optoelectronic devices. Chen, Reed, Schaff, and Eastman (1995) observed that the strain distribution within InGaAs/GaAs QWR of rectangular shape is not uniform, which would contribute to the design of the strained QWR structures. Displacement and strain distribution within QWR were also analyzed by Ulyanenkov, Inaba, Mikulik, Darowski, Omote, Pietsch, Grenzer, and Forchel (2001) using X-ray diffraction. V-shaped [Dupertuis, Oberli, and Kapon (2002)], T-shaped [Grundmann, Stier, and Bimberg (1998)], trapezoidal [Ulyanenkov, Inaba, Mikulik, Darowski, Omote, Pietsch, Grenzer, and Forchel (2001)] and triangular [Gosling and Freund (1996)] QWRs were also studied. So far, however, a rigorous and comprehensive analysis on the induced strain and electric fields is still unavailable.

Under the assumption of isotropic elasticity, Faux, Downes, and O'Reilly (1997) obtained the strain field for both rectangular and crescent QWRs embedded in the full plane. Very recently, Glas (2003) presented results on the strain distribution inside and outside the QWR with the shape of circle, truncated cylinder, and crescent in isotropic semiconductors. Using the conformal mapping method, Ru (2000) derived an analytical solution for QWRs of arbitrary shape within anisotropic piezoelectric media. More recently, Pan (2004) derived an exact closed-form solution for the QWR induced elastic and piezoelectric fields employing the Green's function and equivalent body-force methods. The QWR can be of arbitrary shape and is embedded within the semiconductor half plane with general anisotropic elastic and piezoelectric properties. In a very recent work, Pan and Jiang (2004) showed that material orientation could have a significant influence on the strain and electric distribution inside the trapezoidal QWR.

In this paper, we concentrate on the effect of the QWR shape on the induced elastic and electric fields using the exact closed-form solution derived recently [Pan (2004)]. In what follows, we will give a brief review on this exact solution, and then apply it to the problem involving QWRs with different shapes in the GaAs half-plane structure. Convincing examples are presented to further prove the accuracy and efficiency of the exact solution. Effects of the QWR shapes are revealed and conclusions are drawn which could be important to semiconductor device design.

2 Analytical solution

Let us suppose that there is a general misfit strain γ^*_{Lm} inside the QWR domain V, which is embedded in the z<0 half-plane substrate (Fig. 1). Assuming also that the misfit strain within the QWR is uniform, then the induced field can be found analytically using the Green's function method and the equivalent body-force concept, as has been done recently by Pan (2004). While the detailed derivation can be found in Pan (2004), for the sake of easy reference, we briefly present the main results with definitions for the involved physical quantities. It was shown that the misfit strain-induced elastic displacement and piezoelectric potential can be expressed as an integral on the boundary of the QWR with the Green's function being the integrand [Pan (2004)]:

$$u_K(\boldsymbol{X}) = C_{iJLm}\gamma^*_{Lm}\int_{\partial V} u^K_J(\boldsymbol{x};\boldsymbol{X})n_i(\boldsymbol{x})dS(\boldsymbol{x}) \tag{1}$$

in which $u^K_J(\boldsymbol{x};\boldsymbol{X})$ is the J-th Green's elastic displacement/electric potential at $\boldsymbol{x}$ due to a line-force/line-charge in the K-th direction applied at $\boldsymbol{X}$. C_{iJLm} is the extended material coefficient matrix defined as follows:

$$C_{iJKl} = \begin{cases} C_{ijkl}, & J,K = 1,2,3 \\ e_{lij}, & J = 1,2,3;\ K = 4 \\ e_{ikl}, & J = 4;\ K = 1,2,3 \\ -\varepsilon_{il}, & J = K = 4 \end{cases} \tag{2}$$

where C_{ijkl}, e_{lij} and ε_{il} are the elastic tensor, piezoelectric coefficients, and dielectric tensor, respectively.

For the boundary part made of straight-line segments, the boundary integral can be carried out analytically [Pan (2004)]. Thus, for a QWR with an arbitrary polygonal shape, we sum up the contribution from all the line segments of the QWR boundary. Furthermore, the circular shape can be approximated with piecewise straight-line segments.

Therefore, the final expression of the induced extended displacement due to an arbitrarily polygonal inclusion with N-sides is [Pan (2004)]:

$$u_K(\boldsymbol{X}) = \sum_{s=1}^{N} n_i^{(s)} C_{iJLm}\gamma^*_{Lm}\frac{l^{(s)}}{\pi}\mathrm{Im}\left\{A_{JR}h^{(s)}_R(X,Z)A_{KR} + \sum_{\nu=1}^{4} A_{JR}g^{(s)}_{R\nu}(X,Z)Q^{\nu}_{RK}\right\} \tag{3}$$

where $n_i^{(s)}$ is the i-th outward normal component on the s-th line segment. $l^{(s)}$ is the length of the s-th line segment and can be expressed as $l^{(s)} = \sqrt{(x_2 - x_1)^2 + (z_2 - z_1)^2}$ by setting the generic line segment from point 1 (x_1,z_1) to point 2 (x_2,z_2). In doing so, the outward normal components $n_i^{(s)}$ are constants, given by:

$$n_1^{(s)} = (z_2 - z_1)/l^{(s)};\quad n_2^{(s)} = -(x_2 - x_1)/l^{(s)} \tag{4}$$

Also in Eq. (3), $\boldsymbol{A}$ is the eigenmatrix corresponding to the Stroh eigenvalues p_J given in Ting (1996) and Pan (2004). Matrix $\boldsymbol{Q}$ is defined as:

$$Q^{\nu}_{RN} = B^{-1}_{RS}\overline{B}_{S\nu}\overline{A}_{N\nu} \tag{5}$$

where matrix $\boldsymbol{B}$ is the second eigenmatrix related to the Stroh eigenvalues p_J, with the superscript "-1" denoting inverse matrix, and an overbar the conjugate matrix.

The first term containing h_R in Eq. (3) stands for the contribution from the full-plane Green's function, and the one involving $g_{R\nu}$ for the contribution from the surface boundary condition of the half plane. h_R and $g_{R\nu}$ can be expressed as functions of $\boldsymbol{X}(X,Z)$:

$$h_R(X,Z)=\int_0^1 \ln\{[(x_2-x_1)+p_R(z_2-z_1)]t+[(x_1+p_Rz_1)-s_R]\}dt$$

$$g_{R\upsilon}(X,Z)=\int_0^1 \ln\{[(x_2-x_1)+p_R(z_2-z_1)]t+[(x_1+p_Rz_1)-\overline{s_\nu}]\}dt \tag{6}$$

and eventually have explicit expressions as:

$$h_R(X,Z)=\frac{(x_1+p_Rz_1)-s_R}{(x_2-x_1)+p_R(z_2-z_1)}\ln\left[\frac{x_2+p_Rz_2-s_R}{x_1+p_Rz_1-s_R}\right]+\ln[x_2+p_Rz_2-s_R]-1 \tag{7a}$$

$$g_{R\nu}(X,Z)=\frac{(x_1+p_Rz_1)-\bar{s}_\nu}{(x_2-x_1)+p_R(z_2-z_1)}\ln\left[\frac{x_2+p_Rz_2-\bar{s}_\nu}{x_1+p_Rz_1-\bar{s}_\nu}\right]+\ln[x_2+p_Rz_2-\bar{s}_\nu]-1 \tag{7b}$$

Using the basic strain-displacement and electric field-electric potential relations, the strain and electric fields can be obtained in the exact closed form [Pan (2004)]:

$$\begin{aligned}\gamma_{\beta\alpha}(\boldsymbol{X})=&\sum_{s=1}^{N}0.5n_i^{(s)}C_{iJLm}\gamma_{Lm}^{*}\frac{l^{(s)}}{\pi}\mathrm{Im}\{A_{JR}h_{R,\alpha}^{(s)}(X,Z)A_{\beta R}\}\\&+\sum_{s=1}^{N}0.5n_i^{(s)}C_{iJLm}\gamma_{Lm}^{*}\frac{l^{(s)}}{\pi}\mathrm{Im}\left\{\sum_{\nu=1}^{4}A_{JR}g_{R\nu,\alpha}^{(s)}(X,Z)Q_{R\beta}^{\nu}\right\}\\&+\sum_{s=1}^{N}0.5n_i^{(s)}C_{iJLm}\gamma_{Lm}^{*}\frac{l^{(s)}}{\pi}\mathrm{Im}\{A_{JR}h_{R,\beta}^{(s)}(X,Z)A_{\alpha R}\}\\&+\sum_{s=1}^{N}0.5n_i^{(s)}C_{iJLm}\gamma_{Lm}^{*}\frac{l^{(s)}}{\pi}\mathrm{Im}\left\{\sum_{\nu=1}^{4}A_{JR}g_{R\nu,\beta}^{(s)}(X,Z)Q_{R\alpha}^{\nu}\right\}\end{aligned} \tag{8a}$$

$$\begin{aligned}\gamma_{2\alpha}(\boldsymbol{X})=&\sum_{s=1}^{N}0.5n_i^{(s)}C_{iJLm}\gamma_{Lm}^{*}\frac{l^{(s)}}{\pi}\mathrm{Im}\{A_{JR}h_{R,\alpha}^{(s)}(X,Z)A_{2R}\}\\&+\sum_{s=1}^{N}0.5n_i^{(s)}C_{iJLm}\gamma_{Lm}^{*}\frac{l^{(s)}}{\pi}\mathrm{Im}\left\{\sum_{\nu=1}^{4}A_{JR}g_{R\nu,\alpha}^{(s)}(X,Z)Q_{R2}^{\nu}\right\}\end{aligned} \tag{8b}$$

$$\begin{aligned}E_{\alpha}(\boldsymbol{X})=&-\sum_{s=1}^{N}n_i^{(s)}C_{iJLm}\gamma_{Lm}^{*}\frac{l^{(s)}}{\pi}\mathrm{Im}\{A_{JR}h_{R,\alpha}^{(s)}(X,Z)A_{4R}\}\\&-\sum_{s=1}^{N}n_i^{(s)}C_{iJLm}\gamma_{Lm}^{*}\frac{l^{(s)}}{\pi}\mathrm{Im}\left\{\sum_{\nu=1}^{4}A_{JR}g_{R\nu,\alpha}^{(s)}(X,Z)Q_{R4}^{\nu}\right\}\end{aligned} \tag{8c}$$

3 Numerical analysis

Six different QWR shapes are studied, namely circle, square, downward and upward trapezoids, and downward and upward equilateral triangles (Fig. 1). All QWR shapes are assumed to have the same cross-section area (S= 13.1716 nm^2) and to be located at the same centroid A (0, -4nm) for the purpose of comparison. Furthermore, all QWRs are located symmetrically about the z-axis in the GaAs half plane (z<0) (Fig. 1) and have the same uniform misfit hydrostatic strain in them, i.e., $\gamma_{xx}^{*}=\gamma_{yy}^{*}=\gamma_{zz}^{*}=0.07$.

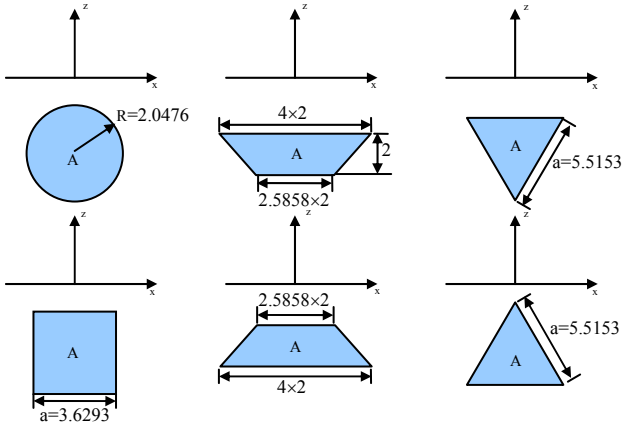

Figure 1: Cross-section parameters of the QWR with six different shapes buried in GaAs substrate (z<0). A (0, -4) is the common geometric center.

The elastic properties for GaAs are C_{11}=118×10^{9}N/m^2, C_{12}=54×10^{9}N/m^2, and C_{44}=59×10^9 N/m^2 [Pan (2002a, b)]. The piezoelectric and relative dielectric constants for GaAs are, respectively, e_{14}=-0.16C/m^2 and ε_r=12.5 [Pan (2002a, b)]. Two orientations are considered: One is GaAs (001) in which the global coordinates *x*, *y*, and *z* are coincident with the crystalline axes [100], [010], and [001], and the other is GaAs (111) where the *x*-axis is along [11-2], *y*-axis along [-110], and *z*-axis along [111] directions of the crystalline [Pan (2002a, b)]. The boundary condition on the surface of the substrate is assumed to be traction-free and insulating [Pan (2002a, b)].

The QWR shape effect on the surface field of GaAs substrate is investigated first as shown in Fig. 2-Fig. 3. Figure 2 (a) shows the hydrostatic strain $\gamma_{xx}+\gamma_{zz}$ along the free surface (z=0) of the substrate GaAs (001), whereas Fig. 2 (b) plots that of the substrate GaAs (111). What these two figures have in common is the sequence of the peak values of QWR for different shapes, i.e. upward triangle has the largest peak value, followed by circle and square with almost the same value; Downward triangle comes after, followed by upward and downward trapezoids (substrate GaAs (001) in (a) and substrate GaAs (111) in (b)). Another interesting point is that along the free surface the hydrostatic strains of circle and square are almost the same, and it is also the case for both upward and downward trapezoid QWRs, where only slight difference can be seen in the middle. This implies that in terms of the induced elastic fields along the surface square is almost identical to circle, and so is the downward trapezoid to upward trapezoid. Looking into details of Fig. 2 (a) we find that the maximum value for different QWRs are all reached in the middle, with a maximum value of 0.35 induced by the upward triangle, which is ½ of the misfit strain. Notice also that in Fig. 2(a) all the curves are symmetric about the middle point *x*=0, as expected in

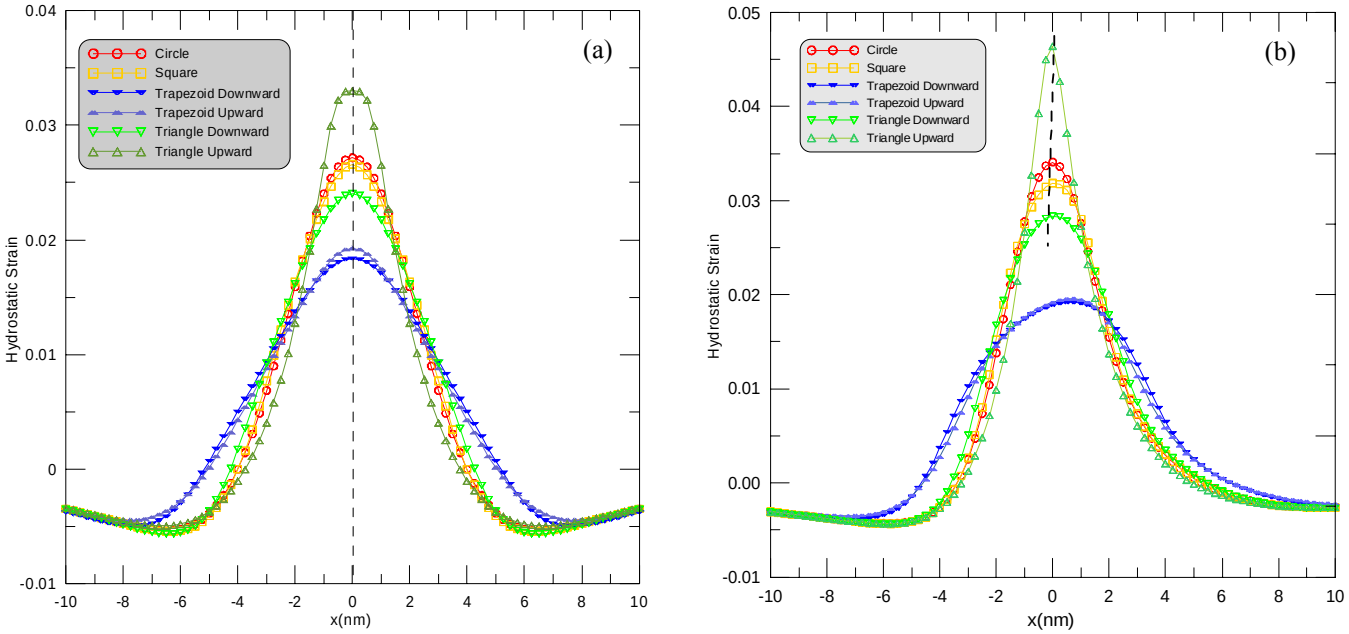

Figure 2: Hydrostatic strain $\gamma_{xx}+\gamma_{zz}$ along the free surface of the substrates induced by the six different QWRs. Substrates GaAs (001) in (a) and GaAs (111) in (b).

GaAs (001). Comparing the hydrostatic strain cases of GaAs (001) and GaAs (111), we further notice that while there is an obvious symmetry with respect to the z-axis for the case of GaAs (001), the strain field in GaAs (111) is no longer symmetric which is clearly due to the effect of material orientation. Furthermore, the magnitude of the strain field is also altered as the orientation changes, with the peak values of hydrostatic strain from different QWRs in GaAs (111) being generally larger than their counterparts in GaAs (001). For instance, the maximum hydrostatic strain in Fig. 2 (b) is roughly 2/3 of the misfit strain, vs. ½ of the misfit strain for the GaAs (001) case (Fig. 2a). It is also interesting to point out that, the induced peak values of the hydrostatic strains from the six different QWRs in GaAs(111) are inclined and are roughly located in the same straight line (Fig. 2(b) dashed line).

The induced total electric field $E=\sqrt{E_x^2+E_z^2}$ ($\times 10^7$V/m) along the free surface of substrate GaAs (111) is shown in Fig. 3. It is already known that for substrate GaAs (001) the electric field is identically zero, thus we only need to study the electric field in GaAs (111) surface. The sequence of the peak electric field for the six different QWRs remains the same as that of the elastic strain field though the trend along the surface tends to be more irregular for the electric field. Again, the maximum values on the surface of GaAs (111) are roughly located along an inclined straight line.

The elastic and electric fields induced within the substrate are plotted in Fig. 4-Fig. 10. Contours of the hydrostatic fields $\gamma_{xx}+\gamma_{zz}$ for the six different QWRs buried in substrate GaAs (001) are first shown in Fig. 4. Generally the hydrostatic value inside the QWR is much larger than that outside. For example, for the circle case the data range inside the QWR is approximately from 0.127 to 0.137, whereas outside the

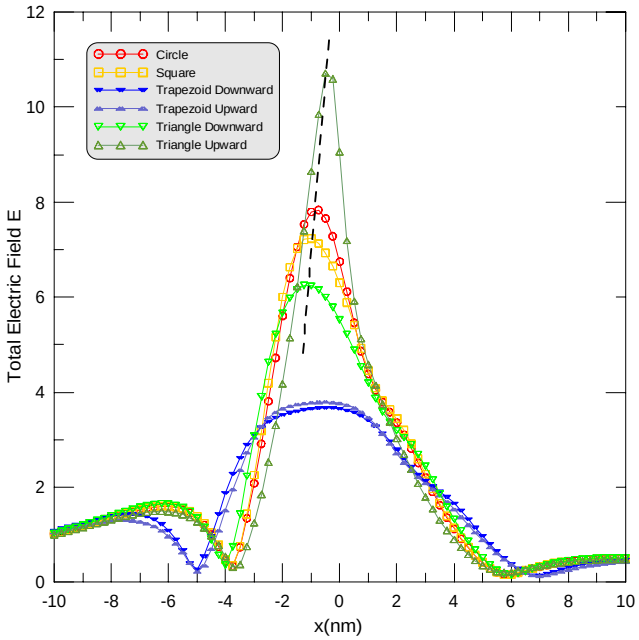

Figure 3: Total electric field $E=\sqrt{E_x^2+E_z^2}$ ($\times 10^7$V/m) along the free surface of substrate GaAs(111) induced by six different QWRs.

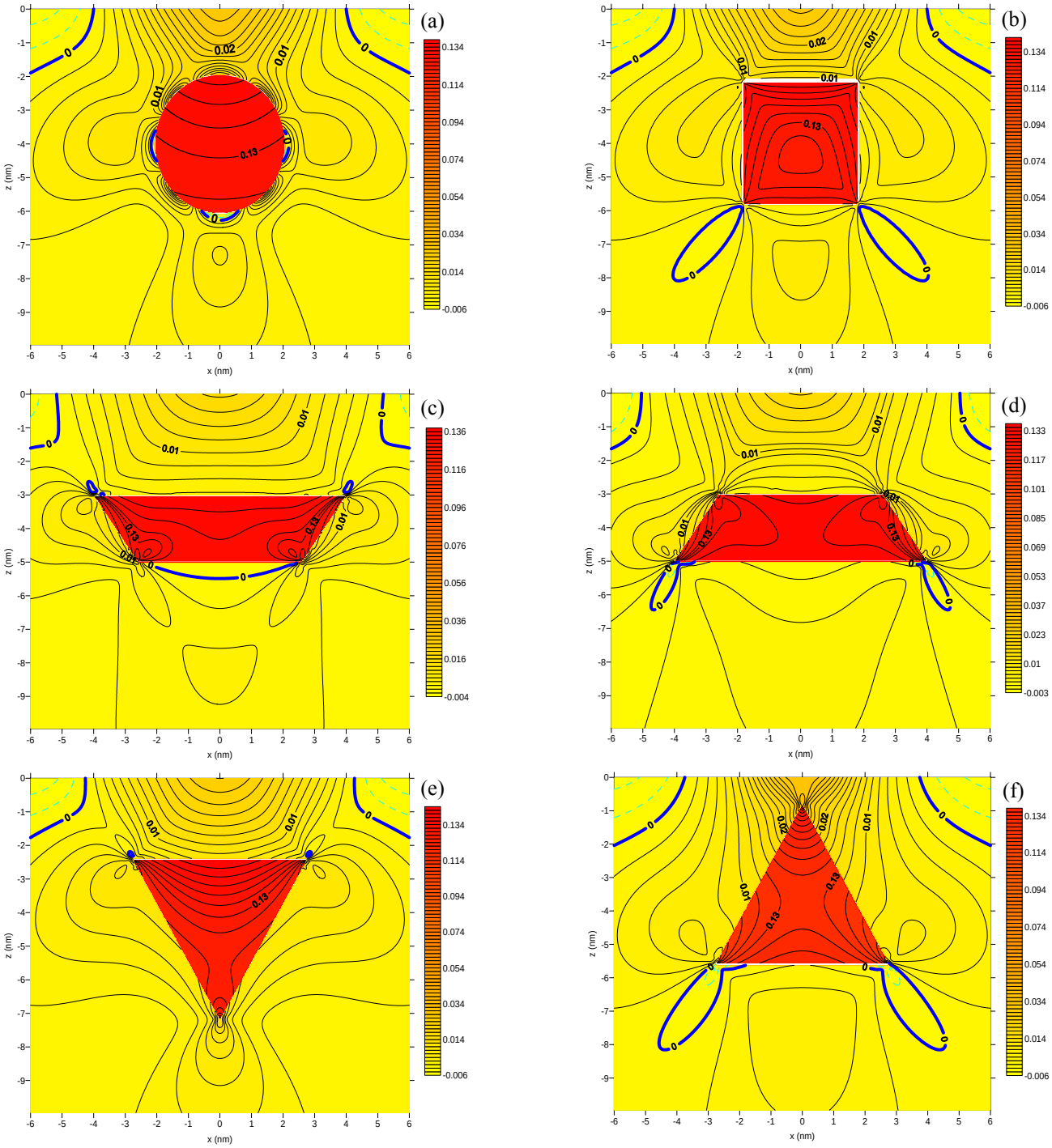

Figure 4: Contours of hydrostatic strain $\gamma_{xx}+\gamma_{zz}$ within GaAs (001) for different QWRs. Circle in (a); square in (b); downward trapezoid in (c); upward trapezoid in (d); downward equilateral triangle in (e); and upward equilateral triangle in (f).

QWR it is roughly from -0.006 to 0.027. A 3D schematic show is given in Fig. 5 (a) & (b) for the circular QWR where the strain differences inside and outside the QWR can be clearly observed. The concentration near the center of the free surface can be also seen from Fig. 5(a), which is consistent with the result shown in Fig. 2(a). We have also marked the zero value with a thick line, which is the interface of the tensile (positive values) and compressive (negative values) domains. In summary, the most striking features of Fig. 4 are as follows:

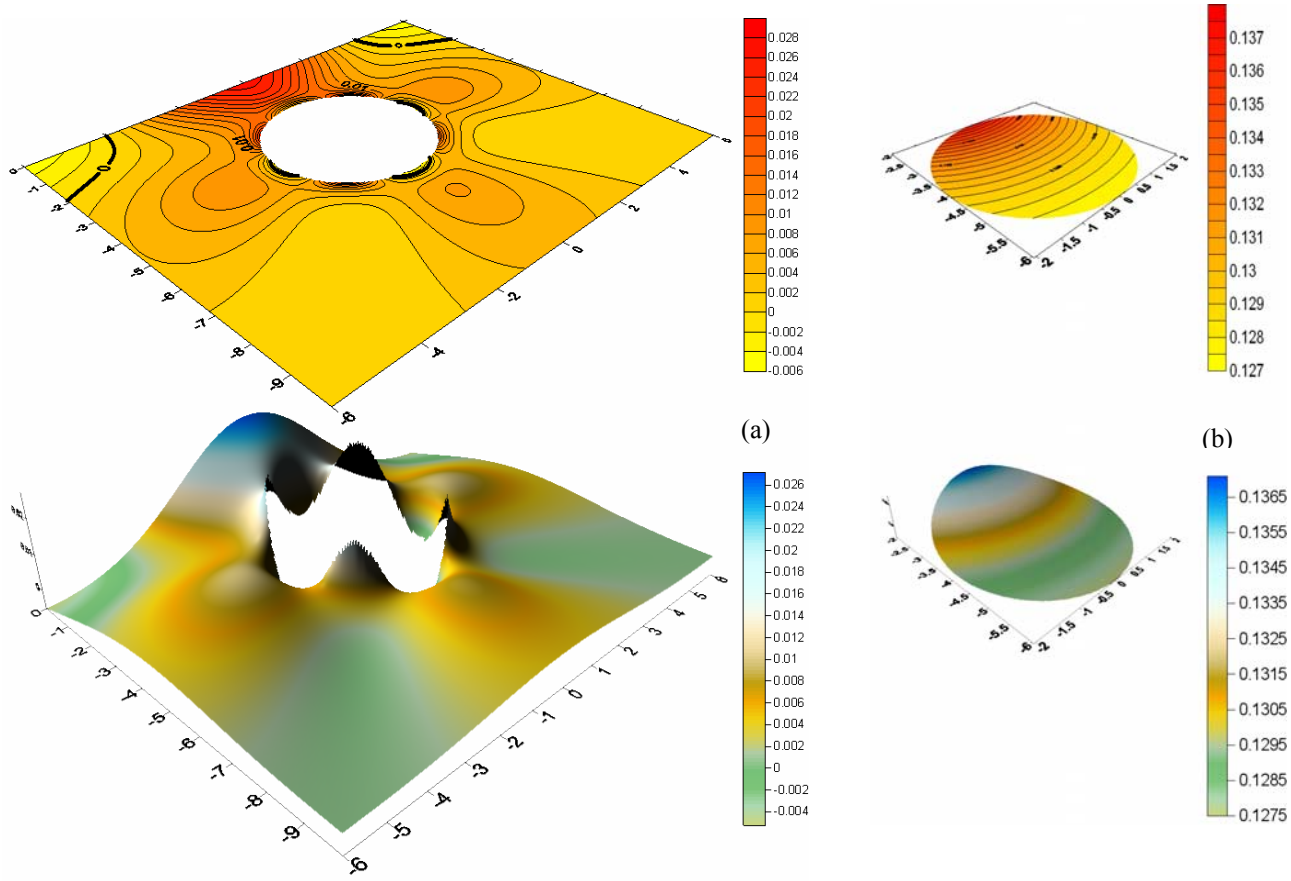

Figure 5: Induced hydrostatic strain $\gamma_{xx}+\gamma_{zz}$ of circular QWR within substrate GaAs (001). (a). within the substrate; (b). within the QWR.

(1) There appears a concentration inside square QWR, which is totally different from the other QWR shapes.

(2) Compared with the data ranges inside QWR of other shapes, more uniform strain distribution inside circle is observed, which might be attribute to the symmetrical nature of the circle shape. The induced strain field within the circle embedded in a full plane is uniform as is well known.

(3) Along the outside boundary of the circle, maximum and minimum values appear alternatively (Fig. 5 (a) & (b)), whilst for other QWRs, there is, in general, a logarithmic singularity at each corner [Pan (2004)].

We also compared our results with some previous ones, e.g. the analytical solution by Glas (2003) for linear isotropic elasticity derived and implemented through an elegant process. Fig. 6(a) and Fig. 7(a) are, respectively, contours of strain components γ_{xx} and γ_{zz} for a circular QWR in GaAs (001) substrate and Fig. 6 (b), Fig. 7(b) are those in GaAs (111) respectively. It is interesting that for GaAs (001), the contour shapes (Fig. 6(a), Fig. 7(a)) are very similar to Glas' isotropic results [Glas (2003)]. However, we also point out that in the inclined case the material orientation would have a significant influence on the induced fields (comparing Fig. 6(a) with Fig. 6(b), Fig. 7(a) with Fig. 7(b)) so that not only the magnitude of the strain field is changed (around 10%) but also the distribution or the shape of the contours both inside and outside QWR is changed with a pronounced loss of symmetry.

Elastic strain field induced by a triangle QWR in GaAs (111) substrate is shown in Fig. 8, which has rarely been studied before. Notice again that the inside value is much larger than that outside the QWR, with the concentration due to the corner singularity. Finally the electric fields within substrate GaAs (111) are plotted in Fig 9 and Fig. 10. Figure 9 illustrates the electric field $E(\times 10^7 \text{V/m})$ induced by the six different QWRs in substrate GaAs (111) where several features are similar to the corresponding elastic strain fields:

1. The electric field inside circular QWR is more uniform than that inside other QWRs;
2. Maximum and minimum values appear alternatively along the outside boundary of circular QWR; but the contours are no longer symmetric due to the change of material orientation (Fig. 9(a), Fig. 10).

Furthermore, the contours of the downward and upward triangles (Fig. 9(e), 9 (f)) are worth of certain detailed discussion: on the side marked with letter A of the triangle

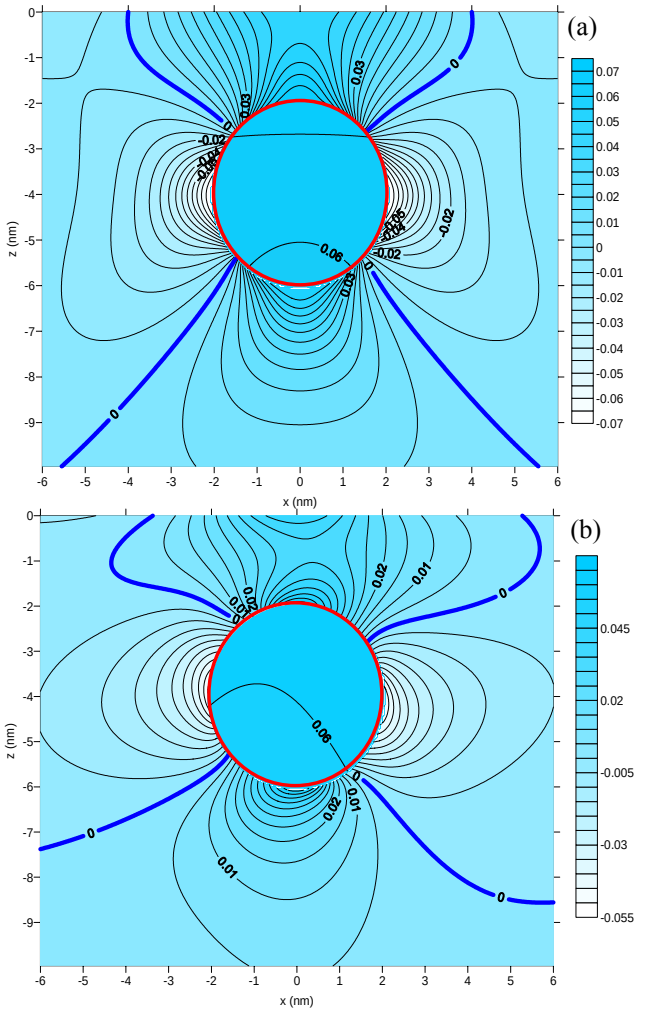

Figure 6: Contours of strain component γ_{xx} of circular QWR within the substrate. (a) and (b) correspond to QWR in GaAs (001) and GaAs (111), respectively.

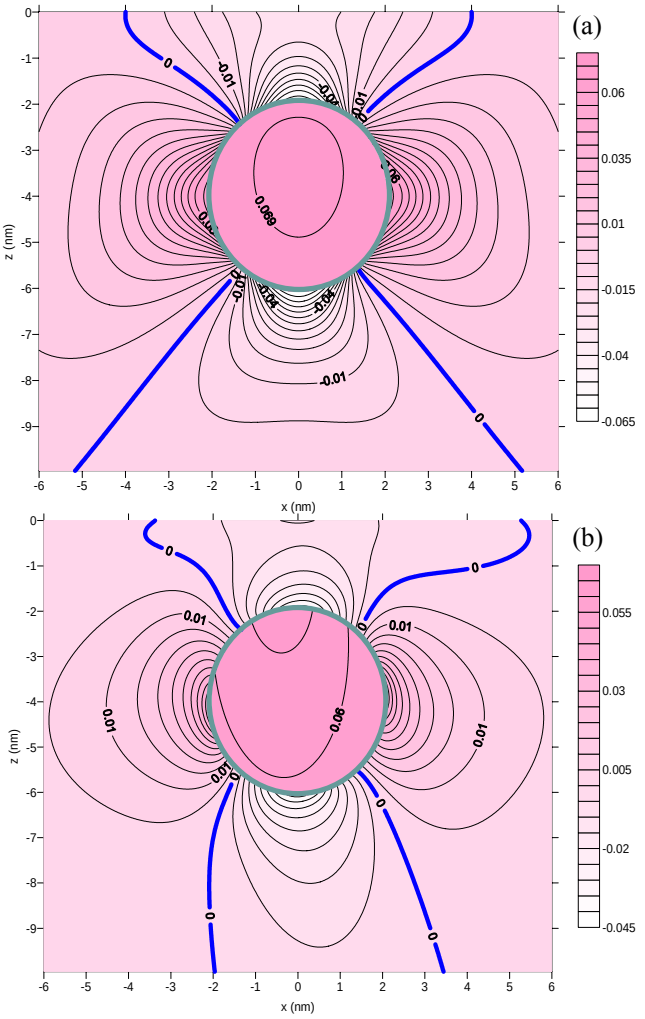

Figure 7: Contours of strain component γ_{zz} of circular QWR within the substrate. (a) and (b) correspond to QWR in GaAs (001) and GaAs (111), respectively.

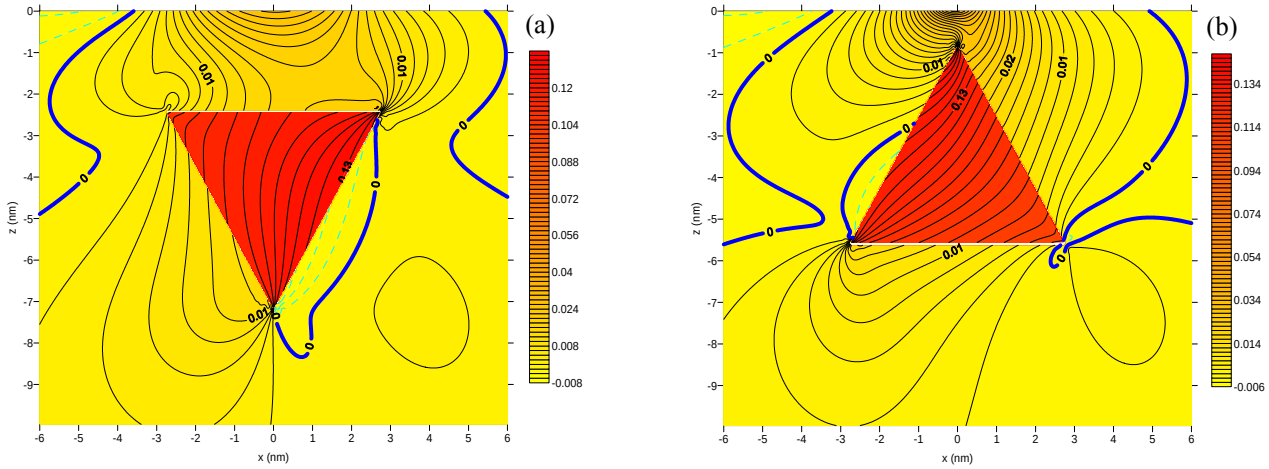

Figure 8: Contours of hydrostatic strain $\gamma_{xx}+\gamma_{zz}$ for the triangular QWR within substrate GaAs (111): downward equilateral triangle in (a) and upward equilateral triangle in (b).

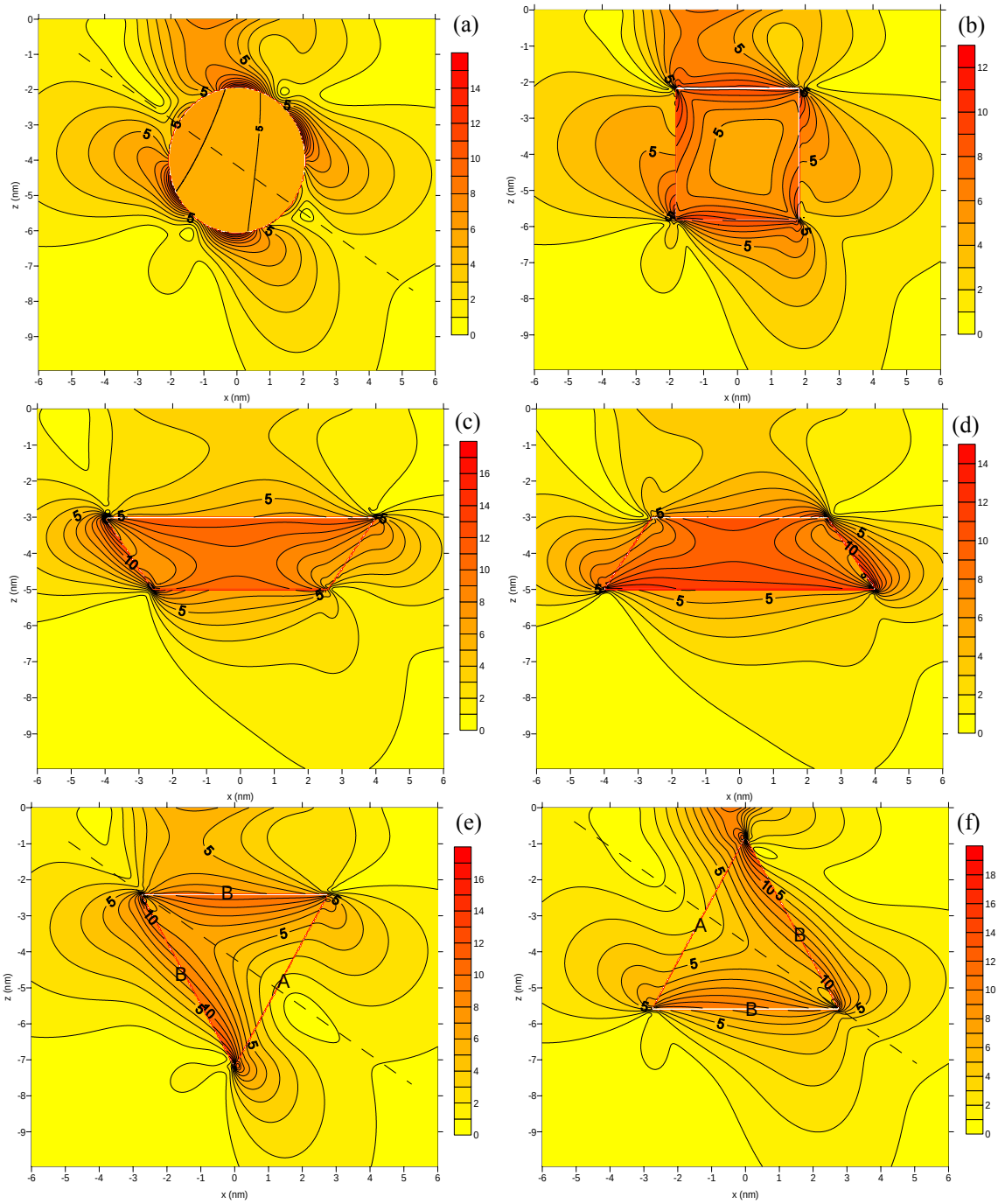

Figure 9: Contours of total electric field $E=\sqrt{E_x^2+E_z^2}$ ($\times 10^7$V/m) within substrate GaAs(111), induced by QWR of different shapes: circle in (a); square in (b); downward trapezoid in (c); upward trapezoid in (d); downward equilateral triangle in (e); and upward equilateral triangle in (f).

the induced electric fields are almost continuous from inside to outside (Fig. 9(e), 9(f)). However on the other two sides marked with letter B, they are completely discontinuous! This feature seems to be associated with the substrate orientation change, and therefore further demonstrates the importance of the material orientation. We also notice that in Fig. 9(e) and (f) the induced electric field is approximately symmetric with respect to a line about 140° to x-axis, (the

dashline in Fig. 9 (e) and (f)), and that for the circular case there are two peak values on each side of this line along the outside boundary of the QWR (Fig. 9(a), Fig. 10).

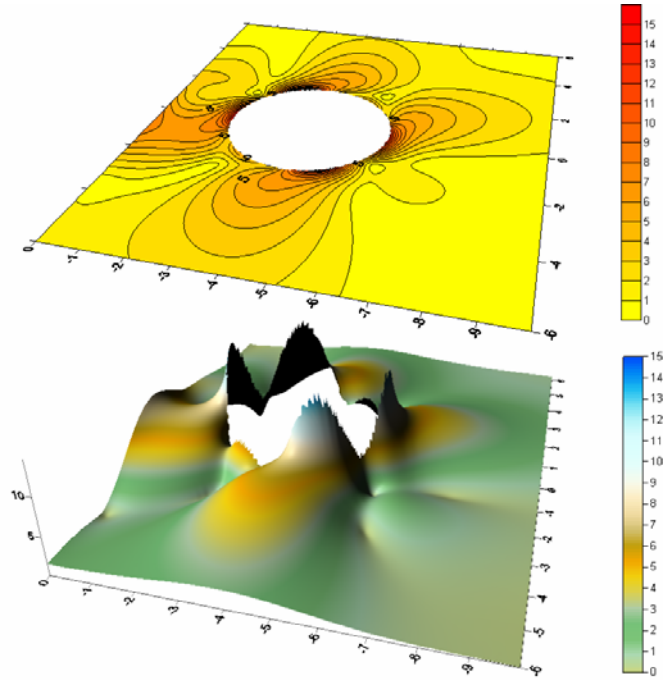

Figure 10: Total electric field $E = \sqrt{E_x^2 + E_z^2}$ ($\times 10^7$V/m) outside circular QWR within substrate GaAs (111).

4 Concluding Remarks

The exact closed-form solution derived recently by Pan (2004) is utilized to solve the QWR induced elastic and electric fields in substrates GaAs (001) and GaAs (111). The induced fields due to six different QWRs, i.e., circle, square, downward and upward trapezoids, and downward and upward equilateral triangles, are examined in certain details. These include the responses along the surface of the substrate, inside the QWR, as well as outside the QWR. From our studies, the following important features are observed:

(1) The elastic and electric fields on the free surface of the half plane are very close to each other for the square and circular QWRs.

(2) The elastic and electric fields within the circular QWR are more uniform than those within QWRs of other shapes.

(3) Concentration near the vertex points of the other-than-circle shapes is clearly observed and therefore sharp corners should be avoided during fabrication.

(4) For the induced hydrostatic strain and total electric fields, a concentration inside the square QWR is observed.

(5) Material orientation plays a very important role in the induced elastic and electric fields.

We finally remark that the results presented are based on the inclusion assumption. That is, the material property within the QWR (of InAs) is the same as its substrate GaAs, following the arguments of Faux, Downes, and O'Reilly (1997). A recent study by Yang and Pan (2002) based on the inhomogeneity assumption (i.e., using the bulk material property of InAs for the QWR and QD) has shown that the magnitude of the induced elastic field could be different from that based on the inclusion assumption, although they share some common features. Therefore, in order to apply the exact closed-form solution presented in this article or the numerical methods developed previously to the practical design of QWR structure, one would need to first determine the material property inside the QWR, which is actually a function of the misfit lattice strain [Ellaway and Faux (2002); Chung and Namburu (2003)]. Investigation on this interesting extension will be reported in the near future.

Acknowledgement The authors would like to express their gratitude to the University of Akron for supporting this work under grant #2-07522, and to the reviewer for constructive comments.

References

Anthony, C. J.; Kelly, M. J. (1994): The effect of cross section on the electron states in quantum wire lasers. *Semiconductor Science and Technology*, vol. 9, pp. 35-40.

Bogachek, E. N.; Scherbakov, A. G.; Landman, U. (1997): Shape effects on conductance quantization in three-dimensional nanowires: Hard versus soft potentials. *Physical Review B*, vol. 56, pp. 1065-1068.

Bolcatto, P. G.; Proetto, C. R. (1999): Shape and dielectric mismatch effects in semiconductor quantum dots. *Physical Review B*, vol. 59, pp. 12487-12498.

Chen, Y. -P.; Reed, J. D.; Schaff, W. J.; Eastman, L. F. (1995): Nonuniform distribution of strain in InGaAs/GaAs quantum wires. *J Vacuum Science Technology B*, vol. 13, pp. 639-641.

Cheong, M. G.; Choi, R. J.; Suh, E. -K.; Lee, H. J. (2003): Bias effect on the luminescent properties of rectangular and trapezoidal quantum-well structures. *Applied Physics Letters*, vol. 82, pp. 625-626.

Chung, P. W.; Namburu, R. R. (2003): On a formulation for a multiscale atomistic-continuum homogenization method. *Int. J. Solids Struct.*, vol.40, pp. 2563-2588.

Constantin, C.; Martinet, E.; Leifer, K.; Rudra, A.; Lelarge, F.; Kapon, E.; Gayral, B.; Gerard, J. M. (2000): Strained V-groove quantum wires in multidimensional microcavities. *Materials Science and Engineering B*, vol. 74, pp. 158-164.

Dupertuis, M. A.; Oberli. D. Y.; Kapon, E. (2002): Computing excitons in V-shaped quantum wires including band-structure and dielectric effects: binding energies and polarization anisotropy of the bright A_1, B_1, A_2 excitons. In: *Technical Proceedings of the Second International*

Conference on Computational Nanoscience and Nanotechnology, pp. 227-230.

Ellaway, S. W.; Faux, D. A. (2002): Effective elastic stiffnesses of InAs under uniform strain. *J of Applied Physics*, vol. 92, pp. 3027-3033.

Faux, D. A.; Downes, J. R.; O'Reilly, E. P. (1997): Analytical solutions for strain distributions in quantum-wire structures. *J Applied Physics*, vol. 82, pp. 3754-3762.

Fu, Y.; Zhao, Q. X.; Ferdos, F.; Sadeghi, M.; Wang, S. M.; Larsson, A. (2001): Strain and optical transition in InAs quantum dots on (001) GaAs. *Superlattices and Microstructures*, vol. 30, pp. 205-213.

Glas, F. (2003): Elastic relaxation of a truncated circular cylinder with uniform dilatational eigenstrain in a half space. *Physica Status Solidi (b)*, vol. 237, pp. 559-610.

Gosling, T. J.; Freund, L. B. (1996): A critical thickness condition for triangular strained quantum wires grown in V-grooves on a patterned substrate. *Acta Materialia*, vol. 44, pp. 1-13.

Grundmann, M.; Stier, O.; Bimberg, D. (1994): Symmetry breaking in pseudomorphic V-groove quantum wires. *Physical Review B*, vol. 50, pp. 14187-14192.

Grundmann, M.; Heitz, R.; Ledentsov, N.; Stier, O.; Bimberg, D.; Ustinov, V. M.; Kop'ev, P.S; Alferov, Zh. I.; Ruvimov, S. S.; Werner, P.; Gosele, U.; Heydenreich, J. (1996): Electronic structures and energy relaxation in strained InAs/GaAs quantum pyramids. *Superlattices and Microstructures*, vol. 19, pp. 81-95.

Grundmann, M.; Stier, O.; Bimberg, D. (1998): Electronic states in a strained cleaved-edge-overgrowth quantum wires and quantum dots. *Physical Review B*, vol. 58, pp. 10557-10561.

Lelarge, F.; Constantin, C.; Leifer, K.; Condo, A.; Lakovlev, V.; Martinet, E.; Rudra, A.; Kapon, E. (1999): Effect of indium segregation on optical properties of V-groove InGaAs/GaAs strained quantum wires. *Applied Physics Letters*, vol. 75, pp. 3300-3302.

Lin, G. (2001): *Studies on Semiconductor Quantum Structure Lasers*. Doctoral Dissertation. National Chiao Tung University, Taiwan, China.

Martinet, E.; Dupertuis, M. –A.; Reinhardt, F.; Biasiol, G.; Kapon, E.; Stier, O.; Grundmann, M.; Bimberg, D. (2000): Separation of strain and quantum-confinement effects in the optical spectra of quantum wires. *Physical Review B*, vol. 61, pp. 4488-4491.

Medeiros-Ribeiro, G. (2002): Epitaxial growth of strained nanocrystals. *Physica Status Solidi*, vol. 230, pp. 443-450.

Notomi, M.; Hammersberg, J.; Weman, H.; Nojima, S.; Sugiura, H.; Okamoto, M.; Tamamura, T.; Potemski, M. (1995): Dimensionality effects on strain and quantum confinement in lattice-mismatched InAsxP1-x/InP quantum wires. *Physical Review B*, vol. 52, pp. 11147-11158.

Ogawa, M.; Itoh, M.; Miyoshi, T. (1996): Analysis of valence-subband structures in a quantum wire with an arbitrary cross-section. *Physica B*, vol. 227, pp.65-68.

Pan, E. (2002a): Elastic and piezoelectric fields around a quantum dot: Fully coupled or semicoupled model? *J Applied Physics*, vol. 91. pp. 3785-3796.

Pan, E. (2002b): Elastic and piezoelectric fields in substrate GaAs (001) and GaAs (111) due to a buried quantum dot. *J Applied Physics*, vol. 91, pp. 6379-6387.

Pan, E. (2004): Eshelby problem of polygonal inclusions in anisotropic piezoelectric full- and half-Planes**.** *J. Mech. Phys. Solids*, (in press).

Pan, E.; Jiang, X. (2004): Analytical study of the elastic and piezoelectric fields in GaAs quantum-wire wtructures. (submitted).

Ru, C. Q. (2000): Eshebly's problem for two-dimensional piezoelectric inclusions of arbitrary shape. *Proc. R. Soc. Lond. A*, vol. 456, pp. 1051-1068.

Shim, H. W.; Choi, R. J.; Jeong, S. M.; Vinh, Le Van; Hong, C. -H, Suh, E.-K.; Lee, H. J.; Kim, Y. –W.; Hwang, Y. G. (2002): Influence of the quantum-well shape on the light emission characteristics of InGaN/GaN quantum-well structures and light-emitting diodes. *Applied Physics Letters*, vol. 81, pp. 3552-3554.

Thilagam, A. (1997): Effect of geometrical shape in the cross section of quantum wires on exciton binding energy. *J Applied Physics*, vol. 82, pp. 5753-5757.

Ting, T.C.T. (1996): *Anisotropic Elasticity*, Oxford University Press, Oxford.

Tsetseri, M.; Triberis, G. P. (2002): A study of the ground state of quantum wires using the finite difference method. *Superlattices and Microstructures*, vol. 32, pp. 79-90.

Ulyanenkov, A.; Inaba, K.; Mikulik, P.; Darowski, N.; Omote, K.; Pietsch, U.; Grenzer, J.; Forchel, A. (2001): X-ray diffraction and reflectivity analysis of GaAs/InGaAs free-standing trapezoidal quantum wires. *J Physics D: Applied Physics*, vol. 34, pp. A179-A182.

Vargiamidis, V.; Valassiades, O. (2002): Shape effects on scattering in three-dimensional quantum wires. *J Applied Physics*, vol. 92, pp.302-309.

Xie, W.; Chen, C. (1999): Size and shape effects of quantum dots on three-electron spectra. *Physica B*, vol. 266, pp. 373-377.

Yang, B.; Pan, E. (2002): Elastic analysis of an inhomogeneous quantum dot in multilayered semiconductors using a boundary element method. *J of Applied Physics*, vol. 92, pp. 3084-3088.